

Nanoscale

Accepted Manuscript



This is an *Accepted Manuscript*, which has been through the Royal Society of Chemistry peer review process and has been accepted for publication.

Accepted Manuscripts are published online shortly after acceptance, before technical editing, formatting and proof reading. Using this free service, authors can make their results available to the community, in citable form, before we publish the edited article. We will replace this *Accepted Manuscript* with the edited and formatted *Advance Article* as soon as it is available.

You can find more information about *Accepted Manuscripts* in the [Information for Authors](#).

Please note that technical editing may introduce minor changes to the text and/or graphics, which may alter content. The journal's standard [Terms & Conditions](#) and the [Ethical guidelines](#) still apply. In no event shall the Royal Society of Chemistry be held responsible for any errors or omissions in this *Accepted Manuscript* or any consequences arising from the use of any information it contains.



Compressed porous graphene particles for use as supercapacitor electrodes with excellent volumetric performance

Huan Li^{a,b,‡}, Ying Tao^{a,b,‡}, Xiaoyu Zheng^{a,b,‡}, Zhengjie Li^{a,b}, Donghai Liu^{a,b}, Zhao Xu^{a,b}, Chong Luo^c, Jiayan Luo^{a,b,*}, Feiyu Kang^c, Quan-Hong Yang^{a,b,c,*}

Received 00th January 20xx,
Accepted 00th January 20xx

DOI: 10.1039/x0xx00000x

www.rsc.org/

This work presents a new class of porous graphene particles with a three-dimensional microscale network and an ultrahigh specific surface area (2590 m² g⁻¹), which is obtained by the KOH activation of a compact graphene hydrogel. As supercapacitor electrodes, such porous graphene particles show high compressibility and little capacitance loss when subjected to a compressive force up to 40 MPa, yielding an excellent volumetric performance with ionic liquid electrolyte. Such carbon materials show great promise for applications needing high volumetric energy.

1. Introduction

Due to its high power density and long life span, the supercapacitor is viewed as a very attractive energy storage device. It usually stores charge through the adsorption of electrolyte ions onto the surface of porous electrodes.^{1,2} Considering the increased requirements for green and portable energy and the limited charge storage ability of supercapacitors, advances have focused on improving their energy density both on a gravimetric and volumetric basis.³⁻⁷ The normally used porous carbon materials for supercapacitors have failed to provide simultaneous high gravimetric and volumetric energy densities because of their low density.⁸⁻¹⁰ A simple but practical method to increase electrode density is the mechanical compression of electrodes made from porous materials that would reduce the volume of unused empty space caused by the poor packing of the material, and consequently increase the volumetric capacitance.^{11,12} However, as a result of the collapse of the porous structure and its accompanying large reduction in specific surface area (SSA), the compressed carbon electrodes always have a limited volumetric

performance. For example, a conventional KOH activation method was recently used to prepare porous graphene sheets with an ultrahigh SSA (up to 3100 m² g⁻¹) with a gravimetric capacitance of 149 F g⁻¹ in an ionic liquid (IL) electrolyte. However, it has a low volumetric capacitance of 54 F cm⁻³ due to the low electrode density (~0.34 g cm⁻³).⁸ After intense compression of such an electrode, the volumetric capacitance is improved to some extent due to the increased electrode density, however, the gravimetric capacitance sharply decreases to 110 F g⁻¹.¹¹ Hence, there is usually a trade-off between compressed density and gravimetric capacitance for most manufactured electrodes. In other words, compression of such a material may not cause an increase in volumetric capacitance. Consequently, it remains a considerable challenge to design electrode materials with a high compressibility that show little gravimetric capacitance loss after compression and thus maximizing volumetric performance.

Assembly of nanomaterials into a compact structure is another effective method to increase electrode density and further increase volumetric performance.¹³⁻¹⁶ We have reported a very dense but porous graphene monolith with a density of up to 1.58 g cm⁻³, which can deliver 376 F cm⁻³ as a supercapacitor electrode in an aqueous electrolyte.¹⁶ However, because of the greater demand for porosity in electrode materials used in an IL electrolyte considering its larger electrolyte ions, it is very difficult to achieve both an increase in material density and volumetric capacitance.¹⁷ Our results show that this very dense carbon possesses a very limited volumetric capacitance of 22 F cm⁻³ in a BMIMBF₄ IL electrolyte (Fig. S1†). The IL is a critically important electrolyte for achieving high safety and a remarkably increased energy density for supercapacitors. This is because it has many merits including a high ionic conductivity, it is solvent free and environmentally friendly, it has a negligible vapour pressure and excellent thermal stability and especially the fact that it has a wide electrochemical window for achieving a high energy density (E∞U²).^{18,19} Apparently, more porosity needs to be introduced into electrode materials for use in an IL electrolyte, but this inevitably decreases the material density.²⁰ To overcome this problem there is an urgent need to develop a new way to balance porosity and density to achieve a high volumetric performance, especially for an IL system.

^aKey Laboratory for Green Chemical Technology of Ministry of Education, School of Chemical Engineering and Technology, Tianjin University, Tianjin 300072, China.

E-mail: qhyangcn@tju.edu.cn; jluo@tju.edu.cn.

^bCollaborative Innovation Center of Chemical Science and Engineering Tianjin 300072, China

^cShenzhen Key Laboratory for Graphene-based Materials and Engineering Laboratory for Functionalized Carbon Materials, Graduate School at Shenzhen, Tsinghua University, Shenzhen 518055, China

†Electronic Supplementary Information (ESI) available. See DOI:

‡These authors are equal main contributors.

Here we present a particle-like form of porous graphene, which we name “porous graphene particles” (PGPs). PGPs are characterized by a particle size of tens of microns and a densely packed structure. They exhibit an ultrahigh specific surface area, up to $2590 \text{ m}^2 \text{ g}^{-1}$ with a three-dimensional (3D) network consisting of activated graphene sheets. PGPs are prepared by KOH activation of a graphene monolith (GM).¹⁶ They can be imagined as the debris from a GM after chemical etching during activation. They inherit the 3D network of the graphene sheets in the parent GM but these are broken into pieces, tens of microns in size, and have large amounts of porosity. Their unique structure gives them a high compressibility, and compressed PGP electrodes can deliver a high volumetric capacitance of 170 F cm^{-3} in 4 V BMIMBF_4 . The corresponding supercapacitors can supply a volumetric energy density as high as 94.6 Wh L^{-1} , which is much higher than for most of the symmetric supercapacitors ever reported.^{8, 11, 12, 15, 16, 21-23}

2. Results and Discussion

2.1 Structure and morphology

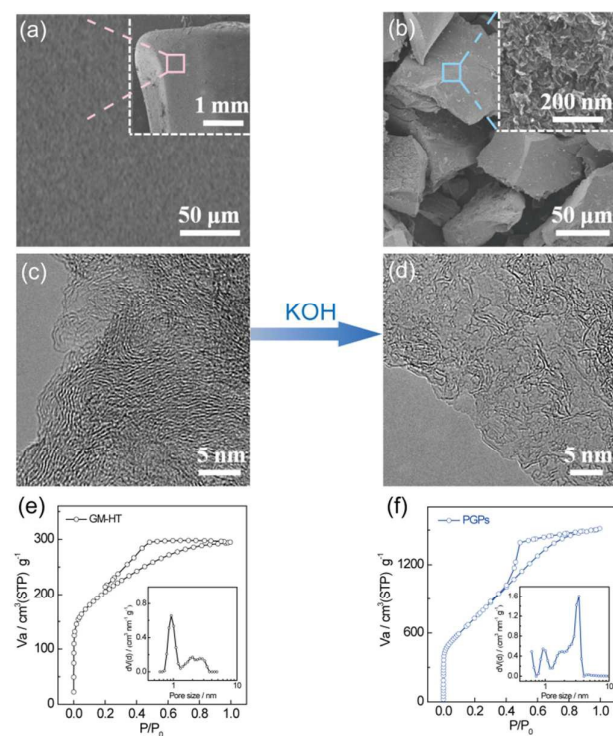


Fig. 1 Comparison between the microstructures of GM-HT and PGPs. SEM images of (a) GM-HT and (b) PGPs; TEM images of (c) GM-HT and (d) PGPs; N_2 adsorption-desorption isotherms and pore size distributions (inset) of (e) GM-HT and (f) PGPs.

As shown in Fig. S2, the preparation of PGPs can be briefly described as follows. A GM hydrogel was prepared by the $180 \text{ }^\circ\text{C}$ 6h hydrothermal reduction of a homogeneous graphene oxide suspension. Then such hydrogel was soaked in a 20 mL KOH solution with different KOH concentration for 12 h static adsorption. Subsequently, a GM hydrogel saturated with a KOH solution was dried under vacuum and the dried sample was heated at $800 \text{ }^\circ\text{C}$ for 1

h under an Ar atmosphere to achieve the chemical activation. Finally bulky GM has broken into PGPs by thoroughly repeated 5 % HCl and diluted water washing to remove residues and drying overnight. A control sample, denoted GM-HT, was prepared by the same process ($800 \text{ }^\circ\text{C}$ heat treatment) but in the absence of KOH, which retains the original shape and morphology of the GM and shows a compact bulk structure (Fig. 1a). The mass ratio of KOH to GM is the key factor that determines the porosity of the activated products. N_2 adsorption/desorption isotherms and the relationship between specific surface area (SSA) and the mass ratio of KOH to GM are given in Fig. S3†. With a KOH to GM mass ratio of 14, the SSA and total pore volume of PGPs can reach $2590 \text{ m}^2 \text{ g}^{-1}$ and $2.15 \text{ cm}^3 \text{ g}^{-1}$ respectively, which is a large increase over that of GM-HT ($720 \text{ m}^2 \text{ g}^{-1}$ and $0.46 \text{ cm}^3 \text{ g}^{-1}$). Scanning electron microscope (SEM) images show that, compared to bulk GM-HT with a very dense structure (Fig. 1a), PGPs (Fig. 1b) have an etched surface but are not broken into isolated graphene sheets after the intense KOH etching involved in activation. They inherit the 3D compact structure of GM-HT and consist of microscopic particles tens of microns in size. Transmission electron microscope (TEM) images show that the PGPs have a porous structure with smaller number of stacked graphene sheets than GM-HT and have a highly wrinkled and interlinked surface (Fig. 1c, d). Pore structure characterization of GM-HT and PGPs was performed by N_2 adsorption/desorption at 77 K . After KOH activation, PGPs show a large increase of SSA and larger volumes of micro- and meso-pores (Fig. 1e, f). Pore size distribution analysis of PGPs determined by the N_2 adsorption/desorption isotherms (Fig. 1f, inset) reveals the presence of $1\text{--}2 \text{ nm}$ micropores with small mesopores around $2\text{--}4 \text{ nm}$. To further demonstrate the microporous structure of PGPs, CO_2 adsorption/desorption data at 273 K was obtained to give insight into its ultra-micro porosity (Fig. 2a). The pore size distribution obtained from CO_2 isotherms confirms the presence of ultramicropores around $0.4\text{--}0.8 \text{ nm}$ in such compact graphene particles (Fig. 2b), which are rarely identified in GM-HT.

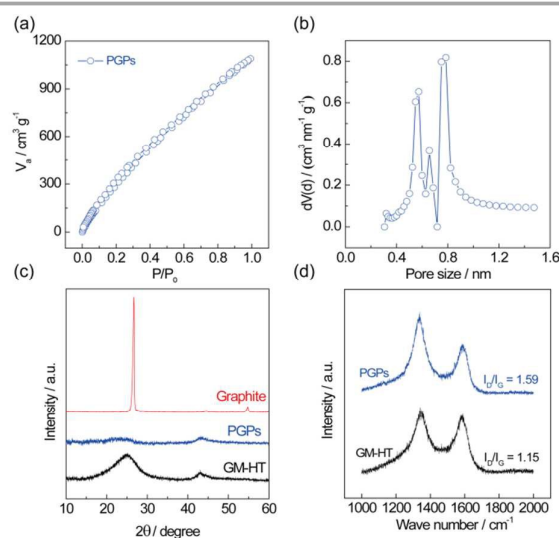


Fig. 2 Structural characterizations. (a) CO_2 adsorption-desorption isotherm of PGPs at 273 K ; (b) Pore size distribution determined by CO_2 isotherm; (c) XRD patterns of graphite, GM-HT and PGPs; (d) Raman spectra of GM-HT and PGPs.

Characterization of PGPs by X-ray diffraction (XRD) and Raman spectroscopy is shown in Fig. 2c and 2d. In the XRD patterns, the (002) peak of PGPs at around 26° has a much reduced intensity and is dramatically broadened, indicating a decrease in the stacking order of the graphene sheets, which is consistent with TEM observations (Fig. 1d). The arrangement of graphene sheets in PGPs is totally different from that in graphite. It is likely that the activated graphene sheets in PGPs interlink to form a porous network structure. Raman spectra of PGPs showed two bands at around 1346 cm^{-1} and 1585 cm^{-1} that are respectively assigned to the D mode corresponding to structural defects and the G mode related to the first-order scattering of the E_{2g} mode observed for sp^2 -carbon domains. The intensity ratio of the D to G bands (I_D/I_G) which is indicative of the degree of disorder of the graphene-based materials, is 1.59 for PGPs compared to 1.15 for GM-HT, demonstrating a much more disordered structure in PGPs. The increased I_D/I_G value confirms the pore evolution after KOH activation.

2.2 Electrochemical performance

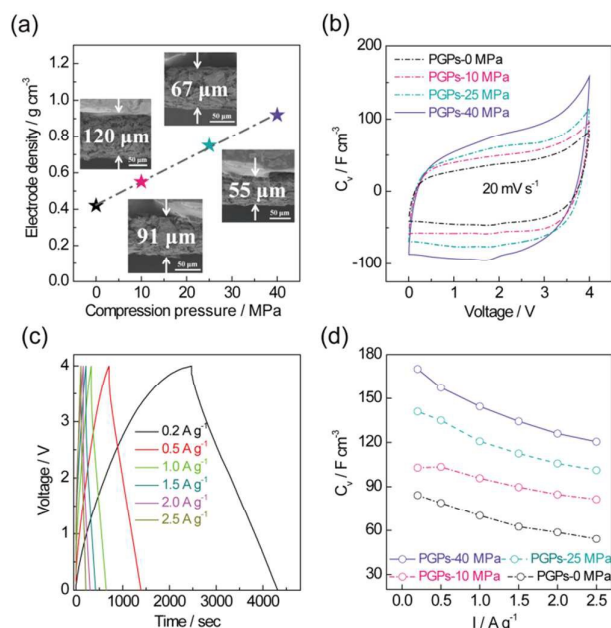


Figure 3 Electrochemical tests of compressed PGPs electrodes. (a) Relationship between compressed electrode density and compression pressure on PGPs electrodes; (b) CV and (c) Galvanostatic charge/discharge curves of PGPs-40 MPa; (d) Rate performance of compressed PGPs electrodes.

As discussed above, PGPs exist as the particles of tens of micrometers and possess ultrahigh surface area with decent amounts of porosity. More importantly, they are not broken into isolated graphene sheets, but exhibit a microscopic compact framework, which fixes their interlinked network and hence contributes to their high compressibility. A compressed PGP electrode is considered to retain its accessible porosity without obvious structural collapse. To evaluate the electrochemical performance of PGPs as supercapacitor electrodes, cyclic voltammetry (CV), galvanostatic charge/discharge and electrochemical impedance spectroscopy (EIS) were carried out

using a symmetrical two-electrode system in a BMIMBF₄ electrolyte. Note that the interlinked graphene network transfers an acceptable conductivity to PGPs. Free of conductive additives, PGPs were mixed with polytetrafluoroethylene as a binding component using a mass ratio of 97:3 for the manufacture of electrodes. After 10, 25 and 40 MPa compression, the electrodes reached densities of $0.55\ \text{g cm}^{-3}$ ($91\ \mu\text{m}$ in thickness), $0.75\ \text{g cm}^{-3}$ ($67\ \mu\text{m}$) and $0.92\ \text{g cm}^{-3}$ ($55\ \mu\text{m}$) respectively, while the electrode density without compression was only $0.42\ \text{g cm}^{-3}$ ($120\ \mu\text{m}$). Depending on the compressive pressure, the electrodes are designated PGPs-0 MPa, PGPs-10 MPa, PGPs-25 MPa and PGPs-40 MPa. It should be noted that when increasing compressing pressure over 40 MPa continuously, the electrode density and porosity remain unchanged. As shown in Fig. 3a, the SEM images of such electrodes show a denser structure with increasing compressive pressure. More importantly, a compressed PGP electrode still shows a 3D porous structure without obvious collapse (Fig. 3a), and retains sufficient accessible micro- and meso-porosity for electrolyte ion adsorption and transport (Fig. S4†). According to Fig. 3b, CV curves of PGPs-40 MPa at a scan rate of $20\ \text{mV s}^{-1}$ from 0–4 V shows a quasi-rectangular shape without any redox peaks, demonstrating efficient electron transport and ion diffusion within such highly compressed electrodes. Galvanostatic charge/discharge curves (Fig. 3c) are nearly linear and symmetrical with small IR drops, demonstrating excellent reversibility, high Coulombic efficiency and small equivalent series resistance (ESR). The excellent capacitive

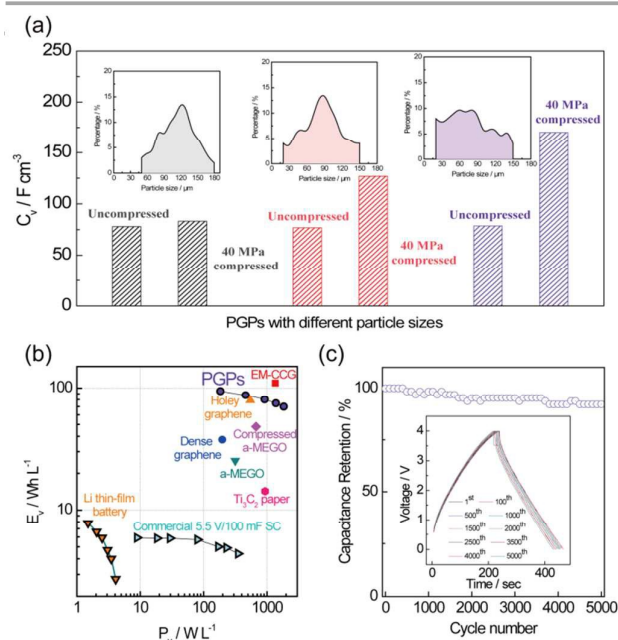


Figure 4 Compression investigations and device performance. (a) The relationship between compressibility (C_v , increasing) and particle size (inset); (b) Ragone plots of compressed PGPs (PGPs-40 MPa) based supercapacitor. The data for Li thin-film battery, Commercial 5.5 V/100 mF SC, Ti_3C_2 paper, a-MEGO, dense graphene, compressed a-MEGO, Holey graphene and EM-CCG are reproduced from ref 23, ref 22, ref 21, ref 8, ref 16, ref 11, ref 12 and ref 15, respectively; (c) Cyclic performance of PGPs-40 MPa based supercapacitors by repeating galvanostatic charge/discharge at $1.5\ \text{A g}^{-1}$ (inset).

performance of such electrodes is also confirmed by the small ESR and charge-transfer resistance in Nyquist plots (Fig. S5†). It is thus not surprising that a highly compressed PGPs-40 MPa electrode has a high volumetric capacitance with excellent rate performance. It has a high C_v value of 170 F cm^{-3} at 0.2 A g^{-1} and 71 % is retained even at a high current density of 2.5 A g^{-1} (Fig. 3d, Fig. S6†). Volumetric capacitance based on compressed electrode density is more evaluable because of the inevitable electrode compression while processing electrode for supercapacitors. But as an important reference, volumetric capacitance based on material density was further studied in Fig. S7†. The compressibility of PGPs can be attributed to their 3D interlinked network on the microscale resulting from the self-assembly process and the extra porosity introduced by activation. After compression, the particles maintain their shape without collapsing and the porosity available inside the particles facilitates charge storage and ion diffusion.

By controlling the KOH mass loading, PGPs with different particle sizes were prepared (Fig. S4†). The particle sizes can be concluded by the statistical results based on several low-magnification SEM images. It was found that the compressed electrode density is largely relevant to the particle size, which can be mainly attributed to the domination of space volumes (Fig. S8†). The relationship between compressibility and particle size of PGPs was further studied to demonstrate their intrinsic compressibility. In Fig. 4a, PGPs-40 MPa with irregular particle sizes together with a higher SSA shows a larger increasing volumetric capacitance (Its detailed electrochemical performance was shown in Fig. 3). While higher SSA contributes to the gravimetric capacitance, the irregular particle size will simultaneously enhance the compressed electrode density and therefore the volumetric capacitance. Moreover, carbon nanotubes (CNTs), hierarchical porous graphene, activated graphene sheets and commercial AC (Fig. S9†) were further compared with PGPs. As shown in Fig. S10†, the compressed PGPs-40 MPa electrode shows only a 10 % gravimetric capacitance (C_s) loss while most of carbon electrodes show a much greater decrease on such high compression (Table S1). Due to the high compressibility of PGPs, a symmetric supercapacitor based on PGPs-40 MPa shows an excellent volumetric performance, which gives a volumetric energy density up to 94.6 Wh L^{-1} and delivers a high power density of 1840 W L^{-1} . The volumetric energy density is much higher than those of most supercapacitors reported previously (Fig. 4b, Table S2). A long cycle life is another critical criterion for supercapacitors in practical applications, and this was evaluated by repeated charge/discharge tests at 1.5 A g^{-1} (Fig. 4c). The capacitance still retained 92 % of its initial value after 5000 cycles, indicating superb electrochemical stability and outstanding reversibility (Fig. S11†).

3. Conclusions

We have introduced a novel class of graphene materials named porous graphene particles (PGPs) produced by the KOH activation of a graphene monolith that can be used for the formation of a compressed electrode. Due to its microscopic particle structure and compact framework of interlinked graphene sheets as well as large amounts of accessible porosity, it shows less capacitance loss after intense compression and hence demonstrates outstanding volumetric

performance. All these features make such porous graphene particles a promising candidate for use in high performance supercapacitors. Our results open up a new avenue for the construction of compressed electrode materials for high volumetric energy storage devices.

Acknowledgments

We thank the financial supports from the National Basic Research Program of China (2014CB932400), National Natural Science Foundation of China (Nos. U1401243 and 51372167), and Shenzhen Basic Research Project (No. ZDSYS20140509172959981 and JCYJ20130402145002430).

Notes and references

1. J. R. Miller and P. Simon, *Science*, 2008, **321**, 651-652.
2. A. G. Pandolfo and A. F. Hollenkamp, *Journal of Power Sources*, 2006, **157**, 11-27.
3. Y. Gogotsi and P. Simon, *Science*, 2011, **334**, 917-918.
4. A. Burke, *Electrochimica Acta*, 2007, **53**, 1083-1091.
5. C. Zhang, W. Lv, Y. Tao and Q.-H. Yang, *Energy Environ. Sci.*, 2015, **8**, 1390-1403.
6. F. Xu; Z. W. Tang; S. Q. Huang; L. Y. Chen; Y. R. Liang; W. C. Mai; H. Zhong; R. W. Fu; D. C. Wu, *Nature Communications* 2015, **6**, 7221.
7. F. Xu; H. Xu; X. Chen; D. C. Wu; Y. Wu; H. Liu; C. Gu; R. W. Fu; D. L. Jiang, *Angewandte Chemie-International Edition* 2015, **54**, 6814-6818.
8. Y. Zhu, S. Murali, M. D. Stoller, K. J. Ganesh, W. Cai, P. J. Ferreira, A. Pirkle, R. M. Wallace, K. A. Cychosz, M. Thommes, D. Su, E. A. Stach and R. S. Ruoff, *Science*, 2011, **332**, 1537-1541.
9. M. F. El-Kady, V. Strong, S. Dubin and R. B. Kaner, *Science*, 2012, **335**, 1326-1330.
10. T. Kim, G. Jung, S. Yoo, K. S. Suh and R. S. Ruoff, *ACS Nano*, 2013, **7**, 6899-6905.
11. S. Murali, N. Quarles, L. L. Zhang, J. R. Potts, Z. Tan, Y. Lu, Y. Zhu and R. S. Ruoff, *Nano Energy*, 2013, **2**, 764-768.
12. Y. Xu, Z. Lin, X. Zhong, X. Huang, N. O. Weiss, Y. Huang and X. Duan, *Nature Communications*, 2014, **5**, 4554.
13. M. Acerce, D. Voiry and M. Chhowalla, *Nature Nanotechnology*, 2015, **10**, 313-318.
14. L. L. Jiang, L. Z. Sheng, C. L. Long and Z. J. Fan, *Nano Energy*, 2015, **11**, 471-480.
15. X. Yang, C. Cheng, Y. Wang, L. Qiu and D. Li, *Science*, 2013, **341**, 534-537.
16. Y. Tao, X. Xie, W. Lv, D. M. Tang, D. Kong, Z. Huang, H. Nishihara, T. Ishii, B. Li, D. Golberg, F. Kang, T. Kyotani and Q. H. Yang, *Scientific Reports*, 2013, **3**, 2975.
17. C. Largeot, C. Portet, J. Chmiola, P.-L. Taberna, Y. Gogotsi and P. Simon, *Journal of the American Chemical Society*, 2008, **130**, 2730-2731.
18. A. B. McEwen, H. L. Ngo, K. LeCompte and J. L. Goldman, *Journal of the Electrochemical Society*, 1999, **146**, 1687-1695.
19. C. Liu, Z. Yu, D. Neff, A. Zhamu and B. Z. Jang, *Nano letters*, 2010, **10**, 4863-4868.
20. C. Long, X. Chen, L. Jiang, L. Zhi and Z. Fan, *Nano Energy*, 2015, **12**, 141-151.
21. M. R. Lukatskaya, O. Mashtalir, C. E. Ren, Y. Dall'Agnese, P. Rozier, P. L. Taberna, M. Naguib, P. Simon, M. W. Barsoum and Y. Gogotsi,

Journal Name

COMMUNICATION

Science, 2013, **341**, 1502-1505.

22. D. Yu, K. Goh, H. Wang, L. Wei, W. Jiang, Q. Zhang, L. Dai and Y. Chen, *Nature Nanotechnology*, 2014, **9**, 555-562.

23. D. Pech, M. Brunet, H. Durou, P. Huang, V. Mochalin, Y. Gogotsi, P.-L. Taberna and P. Simon, *Nature Nanotechnology*, 2010, **5**, 651-654.